Electronic properties of interstitial iron and iron-boron pairs determined by means of advanced lifetime spectroscopy

S. Rein[a] and S. W. Glunz
Fraunhofer Institute for Solar Energy Systems (ISE), Heidenhofstrasse 2, D-79110 Freiburg, Germany

(Received 10 February 2005; accepted 13 September 2005; published online 15 December 2005)

As dissolved iron is one of the most common lifetime-killing contaminants in silicon, its coexisting defect configurations, interstitial iron (Fe_i) and iron-boron pairs (FeB), are investigated on an intentionally iron-contaminated silicon sample by means of temperature-dependent lifetime spectroscopy (TDLS) and injection-dependent lifetime spectroscopy (IDLS). In good agreement with the literature, the study identifies the known Fe_i donor level at $E_t-E_V=(0.394\pm0.005)$eV and determines its symmetry factor as $k=\sigma_n/\sigma_p=51\pm5$, which is an order of magnitude lower than expected from the literature. Using the well-confirmed k factor, the poorly confirmed electron-capture cross section is redetermined as $\sigma_n=(3.6\pm0.4)\times10^{-15}$ cm^2 at 300 K. In addition, the observed exponential $\sigma(T)$ dependence identifies the multiphonon emission mechanism as the dominant capture mechanism for electrons with an activation energy $E_\infty=0.024$ eV. Concerning the defect related to the iron-boron pair, the study unambiguously identifies the deep FeB acceptor level as the dominant FeB recombination center. While the known average value $E_C-E_t=(0.26\pm0.03)$eV for the energy level is well confirmed, the symmetry factor is determined as $k=0.45$, which represents an intermediate value among the scattered results from the literature. Additional spectroscopic information from the defect transformation allows both capture cross sections of the FeB defect to be determined ($\sigma_n=2.5\times10^{-15}$ cm^2 and $\sigma_p=5.5\times10^{-15}$ cm^2). Being suggested as a fingerprint of iron in the literature, the crossover position of the Fe_i- and FeB-dominated IDLS curves (at 300 K) is experimentally proved to be doping dependent which is accurately predicted on the basis of the extracted set of Fe_i and FeB defect parameters. An additional fingerprint of iron is found by the qualitative change of the TDLS curve upon illumination and its S-like shape under dark conditions, which represents a robust criterion for unambiguous identification of iron in silicon. As the most sensitive technique to detect and determine an iron contamination in silicon heavily relies on the Fe_i and FeB defect parameters, the spectroscopic results are of special practical importance. © *2005 American Institute of Physics*.
[DOI: 10.1063/1.2106017]

I. INTRODUCTION

Dissolved iron is one of the most common lifetime-killing contaminants in silicon. In the case of boron doping it may be present as interstitial iron (Fe_i) or iron-boron pairs (FeB), which coexist at room temperature. The technological importance of iron arises, on the one hand, from the many sources of iron contamination during wafer processing and, on the other hand, from the detrimental effect both defect configurations have on the device performance even at very low concentrations. In silicon device technology, considerable interest in the exact recombination properties of the two defect states arises from the fact that the most sensitive technique for detecting an iron contamination and determining its total concentration is based on a quantitative analysis of the well-established difference in the low-injection recombination strength of Fe_i ions and FeB pairs.[1–3] In spite of the intensive studies on iron in the past, there are still relevant defect parameters which are tainted with a high uncertainty.[4,5] To fill this gap, the present study aims at a complete characterization of the Fe_i and the FeB defect by analyzing an intentionally iron-contaminated monocrystalline *p*-type silicon sample by means of advanced lifetime spectroscopy. This technique, which is based on a combination of temperature-dependent lifetime spectroscopy (TDLS) and injection-dependent lifetime spectroscopy (IDLS), has recently been developed[6] and successfully applied to characterize different well-defined impurities in silicon.[7,8] A detailed discussion of the theoretical background and the spectroscopic potential of the different lifetime spectroscopic techniques may be found in Ref. 9, including further details of the iron investigations presented here.

As a starting point, Sec. II provides an overview of the recombination parameters known for the two iron-related defect configurations, taking into account the accuracy of their determination in the literature. After a short discussion of some experimental details in Sec. III, Sec. IV investigates the impact of defect transformation on the temperature- and injection-dependent lifetime measurements and identifies characteristic fingerprints of an iron contamination in silicon. The detailed lifetime spectroscopic investigations to determine the recombination parameters of interstitial iron (Fe_i) and iron-boron pairs (FeB) are presented in Secs. V and VI, respectively. Both studies include a pure TDLS analysis, a

[a]FAX: ++49 761-4588-9250; electronic mail: stefan.rein@ise.fraunhofer.de

TABLE I. Electronic properties of interstitial iron (Fe_i) and iron-boron pairs (Fe_iB_s) in silicon. Values with the label [Av] represent the average values of the results from various techniques and authors, which were published in two review articles. All other values come from original studies using different LS techniques (see *reference list*). The uncertainty in the knowledge of the individual recombination parameters of the two iron defect configurations is indicated by the symbols (see *legend*), which thus reflect the open questions. Reliability is classified as *high* if the results from the literature are consistent and accurate and as *low* if the results from the literature are inconsistent and/or uncertain.

		Capture cross sections					
Defect type	Energy (eV)	σ_p (cm^2)	σ_n (cm^2)	k	E_∞ (eV)	Technique	Reference
Fe_i donor	$E_V+0.38$ [Av]	7.0×10^{-17} [Av]	4.0×10^{-14} [Av]	570	0.045	Average	Istratov *et al.*, 1999 (Ref. 5)
	$E_V+0.39$ [Av]	⋯	⋯	⋯	⋯	Average	Graff 2000 (Ref. 4)
Reliability	high	high	low	low	high		
FeB donor	$E_V+0.10$	2.0×10^{-14}	4.0×10^{-13}	20	⋯	Average	Istratov *et al.* 1999 (Ref. 5)
FeB acceptor	$E_C-0.27$ [Av]	2.0×10^{-15} [a]	1.6×10^{-15} [a]	0.8	⋯	Average	Graff 2000 (Ref. 4)
	$E_C-0.26$ [Av]	3.0×10^{-14} [b]	2.5×10^{-15} [b]	0.08	⋯	Average	Istratov *et al.*, 1999 (Ref. 5)
	$E_C-0.26$ [??]	2.0×10^{-15}	1.6×10^{-15}	0.8	⋯		Zoth and Bergholz, 1990 (Ref. 1)
	$E_C-0.29$	⋯	⋯	⋯	⋯	TDLS	Hayamizu *et al.*, 1991 (Ref. 11)
	$E_C-0.30$	3.0×10^{-14}	2.5×10^{-15}	0.08	⋯	N_{dop}-IDLS	Walz *et al.*, 1996 (Ref. 12)
	$E_C-0.23$	2.0×10^{-15}	3.0×10^{-14}	15	⋯	N_{dop}-IDLS	Macdonald *et al.*, 2001 (Ref. 13)
Reliability	low	low	low	low	⋯		

[a]Values taken from Ref. 1.
[b]Values taken from Ref. 12.

pure IDLS analysis, and a combined analysis of TDLS and IDLS. Finally, the additional information contained in the combined system of the Fe_i- and FeB-dominated IDLS curves is evaluated to gain deeper insight into the recombination parameters of the iron-boron pair. Apart from giving deeper insight into the recombination properties of the iron defects, the study is well suited to further prove the potential of lifetime spectroscopy as a diagnostic tool, as well-known defect parameters will be confirmed.

II. PREVIOUS STUDIES AND AIMS OF THE PRESENT WORK

Table I presents an overview of the recombination parameters determined in the literature for the Fe_i ion and the FeB pair. Apart from average values published independently by Graff[4] and Istratov *et al.*[5] in two recent review articles, the individual results from the few original studies based on lifetime spectroscopy are displayed as well. In order to disclose open questions lifetime spectroscopy may provide answers to, the quality and precision of the individual results are briefly discussed in the following.

A. Electrical properties of the Fe_i defect

Interstitially dissolved iron forms two charge states, a neutral and a positively charged state, which give rise to a single donor level in the lower band-gap half.[5] In numerous studies using DLTS, Hall effect, and electron paramagnetic resonance (EPR), its energy level has been consistently determined as $E_t-E_V=(0.385\pm0.010)$eV.[4,5] The DLTS studies revealed that the hole capture is thermally activated with a barrier energy $E_\infty=(0.045\pm0.005)$eV,[5] which has been confirmed by different authors. This clearly indicates that holes are captured by the Fe_i^0 center via the multiphonon emission mechanism[10] while nothing is known about the capture mechanism for electrons. Concerning the magnitude of the hole-capture cross section of Fe_i, Istratov *et al.*[5] determined an average value of $\sigma_p=7.0\times10^{-17}$ cm^2 at 300 K. This value is highly reliable as it results from a parametrization of the $\sigma_p(T)$ dependence which is based on a least-squares fit of *all* experimental $\sigma_p(T)$ data published to date.[5] By contrast, the electron-capture cross section of Fe_i has been determined less accurately in the literature. Since the average room-temperature value of $\sigma_n=4.0\times10^{-14}$ cm^2 is based on only two studies, it is much less reliable than the value for σ_p. As a consequence, the resulting symmetry factor $k=\sigma_n/\sigma_p=570$ of the Fe_i donor level is tainted with large uncertainty.

Since lifetime spectroscopy allows a direct and accurate k determination, the present study aims at an improved knowledge of both the capture symmetry factor k and the electron-capture cross section σ_n. The quality of the LS result may be assessed from the extracted energy level E_t, which should accurately confirm the average result from the literature. In spite of the intensive studies on the Fe_i defect in the past, it has never been tried to determine its recombination parameters E_t and k by means of lifetime spectroscopy, as far as we know.

B. Electrical properties of the FeB defect

As summarized in Ref. 5, there is strong evidence from various studies using DLTS, Hall effect, EPR, and Fourier transform infrared (FTIR) that the FeB pair in silicon forms three charge states—a neutral, a positively, and a negatively charged state—which give rise to a shallow *donor level* near the valence-band edge and a deep *acceptor level* near the conduction-band edge. While the donor level is known to be located as $E_t-E_V=0.1$ eV,[5] the acceptor level has been determined on average at $E_C-E_t=(0.26\pm0.03)$eV.[5] The few lifetime spectroscopic studies[11–13] already performed on the FeB defect, consistently identified the acceptor level as the dominant recombination center. But as can be seen from the

spectroscopic results compiled in Table I, only the energy level is known with some precision while the results for the capture cross sections and the symmetry factor are inconsistent. These inconsistencies become most noticeable in the reversed capture asymmetry found within the two IDLS studies of Walz *et al.*[12] and Macdonald *et al.*,[13] which most likely arises from a fundamental deficiency of these experiments. Since the Shockley-Read-Hall (SRH) modeling of the IDLS curves had to be based on the combined effect of the FeB acceptor level and the Fe_i donor level, assumptions had to be made for the recombination parameters of the Fe_i donor level which differed in both studies. As the present study reveals the uncertainty in $\sigma_n(Fe_i)$ and $k(Fe_i)$ to be of great significance (see Sec. V), the results obtained from the two IDLS studies for the defect parameters of FeB acceptor level are tainted with this uncertainty and thus limited in quality.

In view of the uncertainties and discrepancies of the results in the literature, the present study aims at a complete characterization of the FeB acceptor level—reducing the assumptions from the literature to a minimum—(i) to prove its dominance as recombination center compared to the FeB donor level and (ii) to elucidate which of its capture cross sections is actually enhanced, i.e., whether $k>1$ or $k<1$.

III. EXPERIMENTAL DETAILS

A. Sample preparation

The investigation has been performed on an intentionally iron-contaminated and boron-doped monocrystalline silicon sample with $[Fe]=2.9\times10^{12}\ cm^{-3}$ and $[B_s]=2.9\times10^{14}\ cm^{-3}$.

Sample preparation in an experiment with the aim of investigating metals in silicon has to ensure that the intentionally introduced impurities (i) remain dissolved to be electrically active and (ii) occur evenly throughout the bulk of the wafer, as this is essential for accurate lifetime measurements.

This may be critical in the case of iron as iron tends to form precipitates due to its high diffusivity and solubility in silicon.[4] The sample investigated here has been manufactured by Wacker Siltronic. For the intentional contamination, elemental iron has been added to the silicon melt before pulling a monocrystalline Czochralski (Cz) silicon crystal. As the number of nucleation centers is reduced to a minimum by a careful control of the pulling conditions and the avoidance of other contaminants than iron in the melt, precipitation is effectively suppressed during crystal growth. Moreover, since outdiffusion during the solidification process is minimized by the small surface/volume ratio of the silicon rod, it is ensured that the iron atoms are incorporated into the silicon lattice and remain dissolved.[14]

Dissolved iron occupies interstitial lattice sites.[4] Since the incorporation during crystal growth is completely determined by segregation, the axial distribution of the final iron concentration can directly be calculated from the metal quantity weighed into the melt using the segregation coefficient known from the literature. For the present sample this led to $[Fe]=2.9\times10^{12}\ cm^{-3}$. Since the axial variation of the impurity concentration over a typical wafer thickness can be neglected, the defect distribution in the wafers finally cut from the crystals is uniform. Thus in terms of both the configuration and the homogeneity of the incorporated iron atoms, the wafers used in the present study are ideally suited for lifetime spectroscopic investigations of the Fe_i and FeB defects.

A further prerequisite for an accurate characterization of bulk defects by means of lifetime spectroscopy is an accurate determination of the bulk recombination properties which in turn requires reducing the impact of surface recombination to such an extent that the measured effective lifetimes, within experimental error, reflect only contributions from the bulk. In the present work this has been achieved by the use of a high-quality silicon-nitride surface passivation whose surface recombination velocity has been determined experimentally as $S<20\ cm/s$ in the whole injection and temperature ranges.[9]

B. Lifetime measurements

For the lifetime measurements two well-established contactless techniques have been applied. While the room-temperature IDLS curves have been measured by means of the quasi-steady-state photoconductance technique (QSSPC),[15] the low-injection TDLS curves have been measured by means of the microwave-detected photoconductance decay technique[16] (MW-PCD) using an integrated liquid-nitrogen-cooled cryostat (for details on the experimental setup see Ref. 9). To guarantee low-injection conditions in the whole temperature range of the TDLS curve, the lifetime measurements have been performed at the minimum bias-light intensity excluding distortions of the monoexponential photoconductance decay due to trapping effects (for details on the experimental procedure see Ref. 9).

IV. DEFECT TRANSFORMATION AND AN ADDITIONAL FINGERPRINT OF IRON IN SILICON

As the two defect configurations of iron (Fe_i and FeB) are metastable, an investigation of their recombination properties requires a detailed knowledge of the defect transformation between the two states. It is well known from the literature[5] that dissociation of the FeB pairs may be induced thermally (at $T>150\ ^\circ C$), optically or by minority-carrier injection, while pair association requires the sample to relax in the dark at temperatures well below 100 °C. To identify the optimum measurement conditions and pretreatments for a TDLS and an IDLS investigation of the Fe_i and the FeB defects, respectively, the impact of temperature and illumination on the injection- and temperature-dependent carrier lifetimes has been studied carefully in a first step.

A. Fingerprint of iron in the injection dependence of carrier lifetime

Concerning the injection dependence of carrier lifetime at room temperature, the impact of light soaking is displayed in Fig. 1. The measurements are performed with the QSSPC technique.[15] Being the stable defect configuration at room temperature, FeB pairs dominate the initial IDLS curve (open circles) which has been measured after a dark storage for 25 h at 50 °C. The observed slight decrease points to-

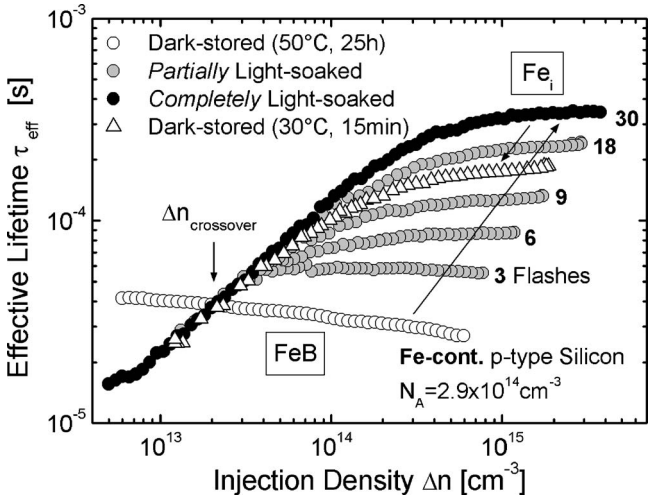

FIG. 1. Effect of light soaking on the injection-dependent carrier lifetime measured by means of the QSSPC technique on an intentionally iron-contaminated boron-doped *p*-type silicon sample ($[Fe]=2.9\times10^{12}$ cm^{-3}, $N_A=[B]=2.9\times10^{14}$ cm^{-3}). The qualitative change of the IDLS curves from a slightly decreasing shape after dark storage for 25 h at 50 °C (*white circles*) to an increasing shape after 30 flashes (*black circles*) originates from optical dissociation of FeB pairs. At the crossover point of the two asymptotic IDLS curves (*black* and *white circles*), carrier lifetime remains unchanged upon defect transformation, which reflects an identical recombination activity of the FeB and the Fe_i defect (at that special Δn).

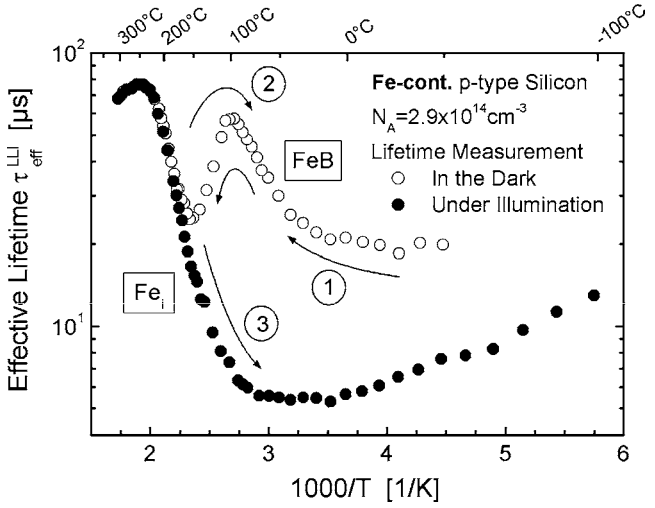

FIG. 2. Effect of light soaking and temperature on the temperature-dependent carrier lifetime under low-level injection measured by means of the MW-PCD technique on the intentionally iron-contaminated *p*-type silicon sample investigated in Fig. 1. If the sample is kept in the dark in between the lifetime measurements, the TDLS curve (*open symbols*) exhibits a peak at 100 °C which is reproduced during ramping up ① and ramping down ②. The unusual lifetime change between 100 and 150 °C may be attributed to thermal dissociation ① (thermal reassociation ②) of FeB pairs. If the sample is illuminated with a maximum bias light ($I_{bias}=0.3$ W/cm^2) in between the lifetime measurements, thermal reassociation of the FeB pairs during ramping down ③ is avoided, the TDLS curve (*closed symbols*) thus reflecting the Fe_i defect.

wards the shallow level expected for the FeB defect. Flashing the sample in between the lifetime measurements with maximum power of the QSSPC flash (peak intensity =25 W/cm^2, decay times=1.9 ms), the IDLS curve becomes steeper with an increasing number of flashes (gray circles). The qualitative change of the IDLS curve directly results from the optical dissociation of FeB pairs. As can be seen, the light-soaked IDLS curves approach an asymptotic shape, which is achieved after 30 flashes (black circles) and mainly reflects the recombination properties of the Fe_i defect. A subsequent storage in the dark again leads to a decrease of the IDLS curve (open triangles) which is induced by a reassociation of FeB pairs.

Comparing the two asymptotic IDLS curves before and after dissociation reveals a characteristic feature of the two iron-related defects, which is well known from the literature.[5] While the Fe_i defect exhibits the higher recombination activity under low-level injection (LLI), the FeB defect does it under high-level injection (HLI). Consequently, dissociation of FeB pairs leads to a lifetime decrease under LLI conditions and to a lifetime increase under HLI conditions. At the crossover point of the two IDLS curves, carrier lifetime remains unchanged upon defect transformation, as the recombination activity of the FeB and the Fe_i defect is the same.

Recently, Macdonald *et al.* suggested the identification of the crossover point as a criterion to detect an iron contamination in silicon.[3] Having investigated iron-contaminated samples with a doping concentration around 10^{16} cm^{-3}, they determined the Δn position of the crossover at 2×10^{14} cm^{-3}.[13] Calculations confirmed this position and led to the postulation that the position of the crossover is independent of the doping concentration as long as $N_A < 1.5\times10^{17}$ cm^{-3}. As the present study on a much lower-doped sample with $N_A=2.9\times10^{14}$ cm^{-3} identifies the Δn position of the crossover at 2×10^{13} cm^{-3} (see Fig. 1), the postulated doping independence of the crossover position proves to be incorrect and with it the set of defect parameters which led to this postulation. On the contrary, combining the observations of both studies, there is experimental evidence that the crossover position increases by an order of magnitude if the doping concentration increases from 2.9×10^{14} to 1×10^{16}. This doping dependence should be reflected by the true set of defect parameters gained from advanced lifetime spectroscopy (see Secs. V and VI).

B. Fingerprint of iron in the temperature dependence of carrier lifetime

Concerning the temperature dependence of carrier lifetime under low-level injection (LLI), the impact of light soaking and temperature is displayed in Fig. 2. The measurements are performed with the MW-PCD technique.[16] If the sample is kept in the dark before (for 25 h at 50 °C) and in between the lifetime measurements, the TDLS curve (open circles) exhibits an unusual S-like shape during ramping up ①, which is reproduced during ramping down ② if the sample is kept in the dark. The unusual lifetime decrease between 95 and 155 °C may be attributed to thermal dissociation ① (thermal reassociation ②) of FeB pairs, as an increasing portion of Fe_i reduces the effective carrier lifetime due to the higher recombination activity of the Fe_i defect under LLI conditions (see previous section). This interpretation is strongly supported by the fact that the S shape completely disappears if the ramping down is not performed in

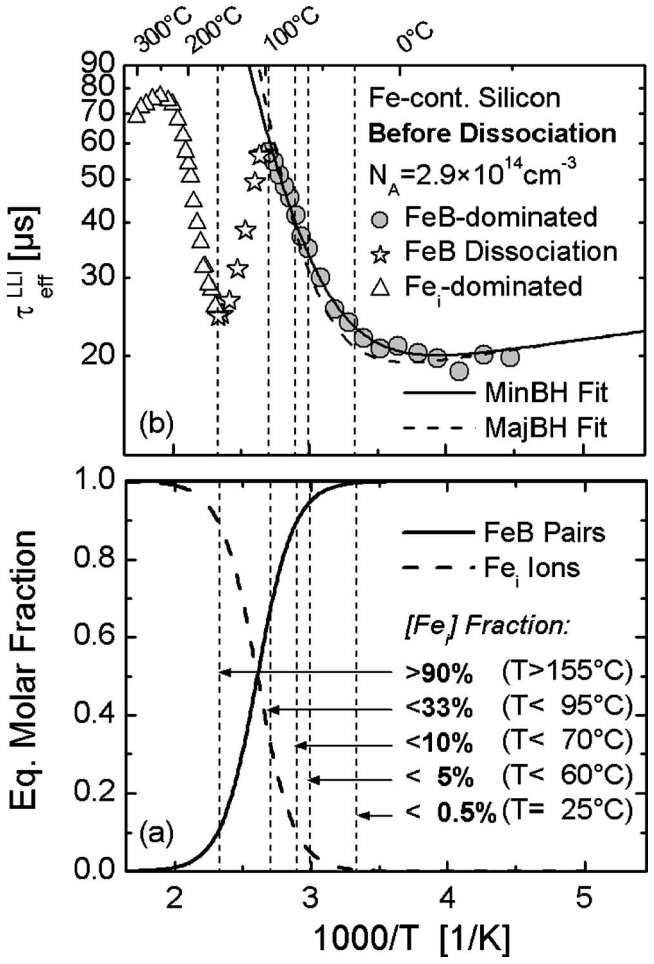

FIG. 3. (a) Equilibrium portions of FeB pairs (*solid line*) and Fe_i ions (*dashed line*) as a function of temperature, only taking into account thermal dissociation. The calculations are based on the empirical Eq. (1) considering the low doping concentration of the sample under investigation. (b) Impact of the thermal dissociation of FeB pairs on the TDLS curve measured in the dark (① in Fig. 2). The *vertical lines* indicate different threshold values of the equilibrium $[Fe_i]$ portion. Being negligible at room temperature, it increases up to 33% at 95 °C (*TDLS peak*) and thus significantly affects the Arrhenius increase of the FeB-dominated part of the TDLS curve (*gray circles*). The one-defect SRH fit of the FeB-dominated part is performed in the T range from −50 to 95 °C for a defect in the upper (MinBH, *solid line*) and the lower (MajBH, *dashed line*) band-gap half on the basis of the advanced T model and σ=const (for discussion see Sec. VI A).

the dark but under strong illumination (I_{bias}=0.3 W/cm^2) in between the lifetime measurements (closed circles). If the dissociation of FeB pairs is stimulated optically, their thermal reassociation below 155 °C can obviously be avoided. It can be concluded that TDLS curve ③ (closed symbols) is dominated by the Fe_i defect in the whole T range. The coincidence of the TDLS curves ① and ③ above 155 °C proves a dominance of the Fe_i defect in that temperature region even under dark conditions.

The above interpretation of the S-like TDLS shape is confirmed by the quantitative analysis shown in Fig. 3. In its lower half the temperature dependence of the equilibrium portions of FeB pairs (solid line) and Fe_i ions (dashed line) is shown. It has been determined from an empirical relation found by Kimerling *et al.*,[17]

$$\frac{[\mathrm{FeB}]}{[\mathrm{Fe}_i]} = C_1 N_A \times \exp\left(\frac{U_1}{k_B T}\right), \tag{1}$$

with $C_1=10^{-23}$ cm^{-3} and U_1=0.65 eV, the low doping concentration N_A of the investigated sample being taken into account. Since the equilibrium portion of Fe_i increases in the T range from 95 °C (TDLS peak) to 155 °C (TDLS valley) from 33% to 90% and since the Fe_i ion is the center of higher recombination activity under LLI conditions, the lifetime decrease observed above 95 °C (open stars) is definitely due to thermal dissociation of FeB pairs. Since the equilibrium portion of Fe_i exceeds 90% above 155 °C, the high-temperature part of the dark TDLS curve (open triangles) definitely reflects the recombination properties of the Fe_i defect. Unfortunately, thermal dissociation not only influences the high-temperature part of the dark TDLS curve. As the equilibrium portion of Fe_i continuously increases from negligible 0.5% at 25 °C to 33% at 95 °C (TDLS peak), it becomes evident that the Arrhenius increase of the FeB-dominated part of the dark TDLS curve (gray circles) is significantly affected by thermal dissociation, which impedes an accurate TDLS analysis of the FeB defect (see Sec. VI).

While the S-like shape of the dark TDLS curves ①② has already been observed in two earlier TDLS studies,[11,18] the qualitative change of the TDLS curves upon illumination has not been reported so far. The qualitative change disproves an interpretation of the S shape given by Kaniava *et al.*[18] They explained the peak around 100 °C by superimposed temperature-dependent carrier trapping and attributed the Arrhenius increase in the high-temperature region to another deep level of the FeB pair, which is not correct (see Fig. 3). The practical importance of the S-shaped dark TDLS curve and the qualitative TDLS change observed upon illumination is that it represents an additional *fingerprint* of an iron contamination. As there is no other contaminant known to show such a behavior, measuring the temperature-dependent lifetime in the dark and under strong illumination provides a very robust criterion to detect iron in silicon.

V. DEFECT CONFIGURATION OF INTERSTITIAL IRON (Fe_i^+)

As the illumination chosen here results in complete optical dissociation of FeB pairs,[3,9] the quantitative spectroscopic analysis of the TDLS and IDLS curves measured after optical dissociation aims at complete characterization of the Fe_i defect. As far as we know, this has not yet been done by means of lifetime spectroscopy.

A. Advanced TDLS analysis

Figure 4(a) displays the TDLS curve ③ (see also Fig. 2), which reflects the recombination properties of the Fe_i defect in the whole T range from 175 to 580 K.[9] As a starting point of the spectroscopic analysis let us first determine the optimum configuration of the SRH model.

While the defect-specific lifetime increase above 330 K arises from the exponential increase of the SRH densities n_1 and p_1,[19] the observed lifetime decrease above 500 K originates from the abrupt onset of intrinsic conduction.[8,9] This

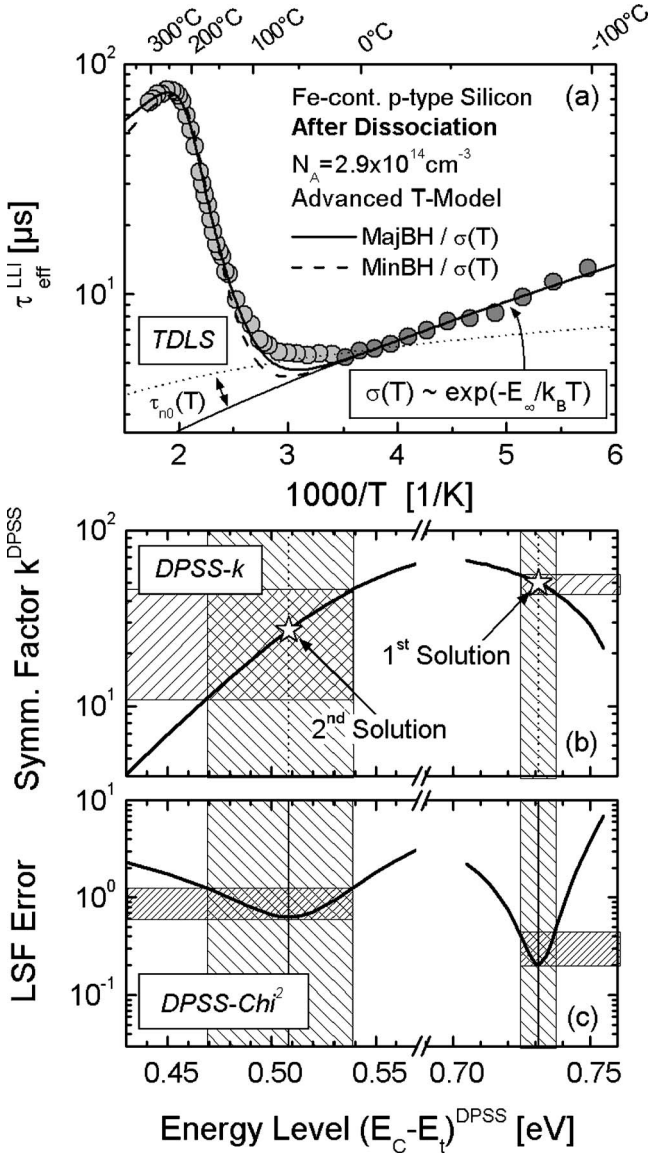

FIG. 4. Advanced DPSS analysis of the Fe_i-dominated TDLS curve ③ taking into account the data in the whole T range (175–580 K). (a) While an accurate modeling below 285 K (*dark gray circles*) requires the insertion of an exponential $\sigma(T)$ model (*thin solid line*), an accurate modeling of the IC-induced TDLS bend above 500 K necessitates the advanced T model. Taking into account both the underlying $\sigma(T)$ model and the advanced T model, the SRH modeling is performed for a MinBH (*dashed line*) and a MajBH defect (*solid line*). [b and c] As the minimum values of the DPSS-chi^2 curve differ significantly, the Fe_i-related defect level is unambiguously localized in the lower band-gap half. The errors of the extracted defect parameters (*shaded areas*) are estimated for tolerated chi^2 values of twice their optimum values.

leads to an exponential increase of the majority-carrier concentration p_0 and thus to a strong reduction of the ratios n_1/p_0 and p_1/p_0 which determine the SRH lifetime under low-level injection in that T region. As can be seen in Fig. 4(a), the high-temperature part of the TDLS curve ($T>500$ K) is well described if the SRH model is based on the advanced T model, which takes into account the temperature dependence of both the equilibrium carrier concentration $p_0(T), n_0(T)$ and the band gap $E_{\text{gap}}(T)$. The chosen models and their implementation are discussed in detail in Refs. 8 and 9. Concerning the low-temperature part ($T<285$ K), an accurate SRH modeling fails for $\sigma=$const (thin dotted line) and requires the introduction of a temperature-dependent capture cross section. Being free of superimposed carrier trapping, the measured TDLS data equal the minority capture time constant $\tau_{n0}(T)=[N_t\nu_{\text{th}}(T)\sigma_n(T)]$ in the T range from 175 to 285 K (dark gray circles), which allows an accurate determination of the underlying $\sigma(T)$ model. The observed $\tau_{n0}(T)$ decrease reflects an exponential increase of the capture cross section with temperature, which can be modeled in terms of $\sigma(T)=\sigma_0\times\exp(-E_\infty/k_BT)$. Fitting this exponential $\sigma(T)$ model to the data (thin solid line), the activation energy of the capture process is determined as $E_\infty=0.024$ eV. The identified $\sigma(T)$ model shows that carrier capture into the Fe_i defect occurs via the multiphonon emission mechanism.[10]

Using the optimum configuration of the SRH model, which takes into account both the underlying $\sigma(T)$ model and the advanced T model, the SRH modeling of the TDLS curve is performed for a defect in the upper (MinBH, dashed line) and the lower (MajBH, solid line) band-gap half, as displayed in Fig. 4(a). To allow a transparent spectroscopic evaluation of the TDLS curves, Figs. 4(b) and 4(c) display the associated defect parameter solution surface (DPSS), which is determined from least-squares SRH fits of the measured TDLS curve for specified but gradually varied energy levels E_C-E_t of the defect center. This evaluation procedure has been introduced in Ref. 7 and is discussed in detail in Ref. 9. Since the DPSS-chi^2 minimum in the MajBH is reduced by more than a factor of 3 compared to the DPSS-chi^2 minimum in the MinBH, the MajBH solution can be identified as the true solution. TDLS alone thus allows a complete characterization of the Fe_i-related defect level, which is localized in the lower band-gap half at $E_t-E_V=(0.393\pm0.005)$eV and found to exhibit a capture asymmetry of $k=50\pm5$. The errors of the extracted defect parameters are estimated from the DPSS diagram tolerating a least-squares error of twice its optimum value [shaded areas in Figs. 4(b) and 4(c)]. As can be seen, both parameters of the MajBH solution are determined with high precision. While the E_t precision is characteristic of any MajBH solution, the precision in the k determination directly results from modeling the distinctive TDLS bend due to intrinsic conduction, which has been measured over a broad T range from 500 to 580 K.[9] As demonstrated in Ref. 9, an accurate modeling of both the low- and high-temperature parts of the TDLS curve is mandatory to obtain an unambiguous spectroscopic result.

B. Advanced IDLS analysis

Although TDLS alone already allowed a complete characterization of the Fe_i defect, the sample has been subject to an IDLS experiment to cross-check the obtained results.

To guarantee a complete dissociation of the FeB pairs, the IDLS curve displayed in Fig. 5 (circles) has been measured after strong optical illumination with 0.1 W/cm^2 for 60 min and is thus dominated by only the Fe_i defect.[3,9] As can be seen from Fig. 5, an accurate SRH modeling (line) of the measured injection dependence is achieved in a broad Δn range from 10^{12}–10^{15} cm^{-3} for a single defect level. Since

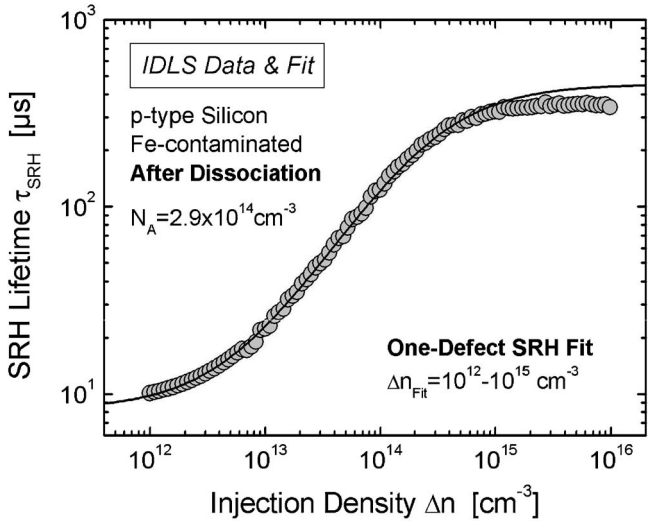

FIG. 5. SRH analysis of the Fe_i-dominated IDLS curve. To ensure a complete dissociation of the FeB pairs, the IDLS curve is measured after an illumination step with a halogen lamp (0.1 W/cm^2, 60 min) (*circles*). An accurate SRH modeling (*line*) is achieved in a broad Δn range of $10^{12}-10^{15}$ cm^{-3} for a single defect level. The associated defect parameter solution surface is shown in Fig. 6 (*dashed line*).

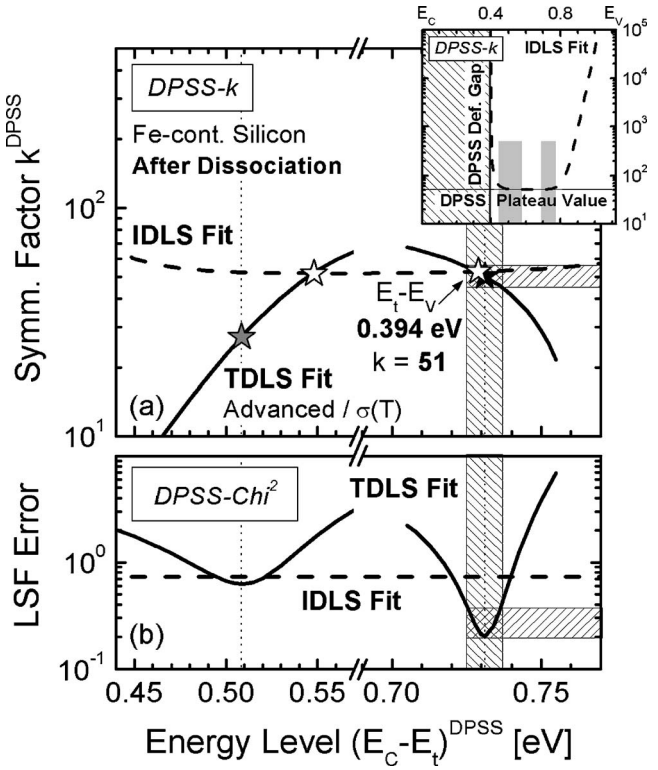

FIG. 6. Superposition of the DPSS diagrams associated with the Fe_i-dominated TDLS (*solid lines*, see Fig. 4) and IDLS (*dashed lines*) curves of the iron-contaminated sample. The global structure of the DPSS-*k* curve related to IDLS is shown on the upper right. The regions which are shown in detail in the superposed DPSS-*k* diagram are indicated by the *gray areas*. Unambiguous determination of the defect parameters of interstitial iron from the intersection point of the DPSS-*k* curves in the MajBH (*white star*). The coincidence of this intersection point with the minimum of the DPSS-chi^2 curve (*gray star*) manifests the accuracy of the determination.

this defect level clearly dominates the whole range of low and medium injection densities, which is the relevant Δn range for a comparison with TDLS, we chose 2×10^{15} cm^{-3} as an upper bound of the fitted Δn range and performed the modeling on the basis of a one-defect SRH model.

Due to the strong inherent ambiguity of the SRH parametrization of a single IDLS curve,[7,8] its detailed spectroscopic evaluation requires determining the associated defect parameter solution surface, which is again determined from least-squares SRH fits of the measured IDLS curve for specified but gradually varied energy levels E_C-E_t of the defect center. The resulting DPSS-*k* curve is displayed in Fig. 6(a) (dashed line). The energy independence of the corresponding DPSS-chi^2 curve, shown in Fig. 6(b), visualizes that the DPSS parameters (E_t,k) represent equivalent solutions for the SRH parametrization of the IDLS curve, which prevents the defect parameters to be determined from only the IDLS curve.

As expected for an increasing IDLS curve,[9] the DPSS exhibits a tublike structure with a continuous range of validity and a definition gap towards the conduction band (dashed area) shown on the top right in Fig. 6(a). The characteristic plateau value of the DPSS-*k* curve per definition represents a lower bound for the true *k* factor of the defect center.[9] The fact that it is determined as $k^{\text{DPSS-PL}}=51.5$ [see Fig. 6(a)] definitely proves a capture asymmetry for the Fe_i-related defect level.

C. Combined DPSS analysis of TDLS and IDLS

To verify the consistency of the spectroscopic results obtained from the IDLS and the TDLS analyses, the associated DPSS diagrams simply have to be superposed, as shown in Fig. 6.

Although the intersection points (white stars) of the two DPSS-*k* curves associated with TDLS (solid lines) and IDLS (dashed lines) reflect consistent parameter solutions, their quality significantly depends on their energy distance from the corresponding minimum of the DPSS-chi^2 curve related to TDLS, which reflects the varying accuracy of the solutions contained in the DPSS-*k* curve associated with TDLS. The exact coordinates of the DPSS-*k* intersection points are given in Table II in comparison with the spectroscopic results obtained from the isolated analyses of TDLS and IDLS.

Since the DPSS-*k* intersection point in the lower band-gap half deviates in its energy position 40 meV from the corresponding DPSS-chi^2 minimum, it has to be rejected for reasons of inconsistency, which demonstrates in accordance with the reduced fit quality of the TDLS MinBH solution (see Sec. V A) that the Fe_i-related defect level cannot be located in the upper band-gap half. In the lower band-gap half, on the contrary, the energy positions of both the DPSS-*k* intersection point and the minimum of the DPSS-chi^2 curve perfectly coincide, which proves the finding from TDLS that the Fe_i-related defect level is located in the lower band-gap half. From the DPSS-*k* intersection point (white star) the energy level and the symmetry factor of the Fe_i defect are determined as $E_t-E_V=0.395$ eV and $k=53$, respectively, which well confirms the results obtained from TDLS alone (gray star).

TABLE II. Overview of the spectroscopic results obtained for the Fe_i defect by investigating the iron-contaminated sample with the different LS techniques: TDLS alone (see Fig. 4), IDLS alone (see Fig. 5), and the combination of TDLS and IDLS (see Fig. 6). The final LS result is shown in the last row of the table.

		MinBH defect		MajBH defect	
Technique	Boundary condition	E_C-E_t (eV)	k	E_t-E_V (eV)	k
TDLS	Advanced/$\sigma(T)$	0.509 (0.47-0.54)	27.2 (11-46)	0.393 (0.40-0.39)	50.1 (45-55)
IDLS	One-defect fit	0.509 (E_t^{TDLS})	52.2	0.393 (E_t^{TDLS})	52.7
IDLS and TDLS	DPSS-IP	0.548	51.6	0.395	52.5
Final result		···	···	0.394±0.005	51±5

As the DPSS-k intersection point is located in the flat plateau region of the DPSS-k curve related to IDLS, its energy position is mainly determined from TDLS whereas its k value mainly results from IDLS. Being aware of the fact that TDLS alone precisely determined the symmetry factor for the MajBH solution as $k=50$ (see Sec. V A), this observation reveals that the k factor has been reproduced by two independent techniques, TDLS and IDLS, which proves the high reliability of the obtained result. Averaging the defect parameters obtained from TDLS alone (gray star) and the combined analysis of TDLS and IDLS (white star), the Fe_i defect is localized in the lower band-gap half at $E_t-E_V=(0.394\pm0.005)$eV with a symmetry factor $k=51\pm5$.

D. Comparison of the LS results with the literature and discussion

In agreement with the results from the literature which have been summarized in Sec. II A, lifetime spectroscopy identified the Fe_i-related donor level in the lower band-gap half. Concerning the energy level E_t, the determined value of $E_t-E_V=(0.394\pm0.005)$eV is in excellent agreement with the average value of $E_t-E_V=(0.385\pm0.010)$eV found in the literature[4,5] (see Sec. II A). Taking into account that the energy level of the Fe_i defect is the best-determined Fe_i parameter in the literature and considering that the energy level is the only defect parameter that *both* techniques, LS and DLTS, are capable of determining with high accuracy, the coincidence of the E_t results from LS (present study) and DLTS (literature) demonstrates the high reliability of the LS result.

However, concerning the symmetry factor k, the determined value of $k=51\pm5$ is more than an order of magnitude lower than the value of $k=570$, which can be calculated from the capture cross sections known from the literature (see Sec. II A). In spite of this strong deviation, the LS result is believed to be more reliable than the DLTS-based result from the literature. From a general point of view this is due to the fact that LS sensitively depends on k and thus allows a direct access. DLTS, on the contrary, only allows an indirect access via the capture cross sections and faces the problem that the σ determination is tainted with a relatively large uncertainty. Apart from these theoretical aspects, the LS result has to be favored in terms of experimental reproducibility. While the measured k value has been precisely reproduced by two independent LS techniques (see Sec. V C), the calculated k value had to be based on σ_n results from the literature which are poorly confirmed and therefore uncertain (see Sec. II A). The symmetry factor k thus being well determined from lifetime spectroscopy but significantly changed compared to the literature, recalculating the electron-capture cross section σ_n to remove the existing uncertainty suggests itself. Using for the hole-capture cross section the well confirmed average value of $\sigma_p=7.0\times10^{-17}$ cm^2 (at 300 K) and calculating the product $\sigma_n=k\times\sigma_p$, we find for the electron-capture cross section of the Fe_i donor level a value of $\sigma_n=(3.6\pm0.4)\times10^{-15}$ cm^2 (at 300 K).

In agreement with the results from the literature, TDLS revealed an exponential T dependence of the capture cross section which shows that carrier capture into the Fe_i donor level occurs via the multiphonon emission mechanism. However, the activation energy of the capture process has been determined as $E_\infty=0.024$ eV and is thus found to be slightly reduced compared to the value of $E_\infty=0.043$ eV reported in the literature.[4] As the $\sigma(T)$ results in the literature come from standard DLTS, they refer to the hole (majority) capture cross section σ_p, whereas the $\sigma(T)$ results from TDLS actually refer to the electron (minority) capture cross section σ_n. Thus the observed deviation in E_∞ might indicate that even though the T models of the two capture cross sections are identical in terms of their qualitative structure, they may slightly differ in terms of their activation energy E_∞. However, as the Fe_i donor level is located in the lower band-gap half, a difference in the $\sigma(T)$ models would not affect the TDLS modeling as discussed in Ref. 9. Experimentally, this is clearly shown by the self-consistency of the obtained lifetime spectroscopic results.

VI. DEFECT CONFIGURATION OF IRON-BORON PAIRS (FeB)

After the successful characterization of the Fe_i defect, the following section focuses on the characterization of the defect related to iron-boron pairs (FeB), the TDLS and IDLS curves measured after dark storage being analyzed. The equilibrium calculations in Sec. IV B already disclosed the fundamental problem of this analysis in the present case. Even ideal dark-storage conditions only ensure complete pairing of iron at room temperature, while above room temperature a significant impact of thermal dissociation cannot be avoided. Although IDLS alone thus allows accurate spectroscopic analysis of the FeB defect, a significant delimitation of the FeB recombination parameters may already be achieved by a rather qualitative analysis of the TDLS curve.

A. TDLS analysis

As the FeB-dominated part of the dark TDLS curve (gray circles) is affected by an increasing equilibrium portion of Fe_i, a one-defect SRH modeling in the T range from −50 to 95 °C, as shown in Fig. 3(b) for a MinBH (solid line) and a MajBH defect (dashed line), only allows the FeB defect parameters to be estimated qualitatively. If thermal dissociation is neglected up to 95 °C, TDLS determines the FeB level either as $E_C-E_t=0.26$ eV or as $E_t-E_V=0.34$ eV. Since the least-squares error of the fit is almost an order of magnitude lower for the MinBH solution than for the MajBH solution, a localization of the FeB level in the upper band-gap half is likely (for the detailed DPSS analysis see Ref. 9).

The systematic error of this result which arises from the interference by Fe_i may be estimated by a simple consideration. As the Fe_i defect is the center of higher recombination activity under LLI conditions, its increasing portion leads to an Arrhenius increase with reduced slope and thus results in an underestimation of the FeB energy depth, if affected T regions are included in the fit. If the upper T bound is reduced from 95 to 60 °C, which corresponds to a significant reduction of the tolerated Fe_i portion from 33% to 5%, the energy depth of the MinBH solution, in fact, increases from 0.26 to 0.29 eV, being accompanied by an increase of the k factor from 0.07 to 0.5. The energy depth of the MajBH solution, on the contrary, remains almost unchanged and is determined in both fits around 0.34 eV. The observed insensitivity towards variations of the fitted T range directly results from the fact that the position of the Arrhenius increase only depends on the energy level E_t but not on the symmetry factor k in the case of a MajBH defect.[9] This implies that only the modeling of the onset region already allows a relatively robust E_t determination. In the present case this observation gains special importance as the onset region of the Arrhenius increase is observed below 50 °C, which ensures that it is almost unaffected by thermal dissociation and thus purely reflects the properties of the FeB level.

In spite of an increasing modeling uncertainty with decreasing width of the Arrhenius increase, the TDLS results obtained from the modeling on the reduced T range allow narrowing down of the recombination parameters expected for the FeB defect. (i) Band-gap half: The relevant band-gap half may be identified by comparing the energies of the MinBH and MajBH solutions in terms of their magnitude with the energies of the two eligible FeB defect levels known from the literature: the donor level at $E_t-E_V=0.1$ eV and the acceptor level at $E_C-E_t=(0.26\pm0.03)$eV (see Table I). As the energy depth of the MajBH solution is determined with high reliability to be as deep as 0.34 eV, the shallow donor level can definitely be excluded as dominant recombination center, which unambiguously identifies the upper band-gap half to be relevant. (ii) Energy depth: This is further supported by the fact that the energy depth found for the MinBH solution varies between 0.26 and 0.29 eV, which nicely coincides with the energy interval from 0.23 to 0.29 eV known for the acceptor level. However, the TDLS modeling suggests the acceptor level to be located rather in the upper than in the lower half of the E_t interval from the literature. (iii) k-factor: Finally, the detailed DPSS analysis in Ref. 9 shows that even at the upper bound of the uncertainty interval for k, TDLS unambiguously suggests a symmetry factor $k<1$, i.e., an enhancement of the hole capture compared to the electron capture.

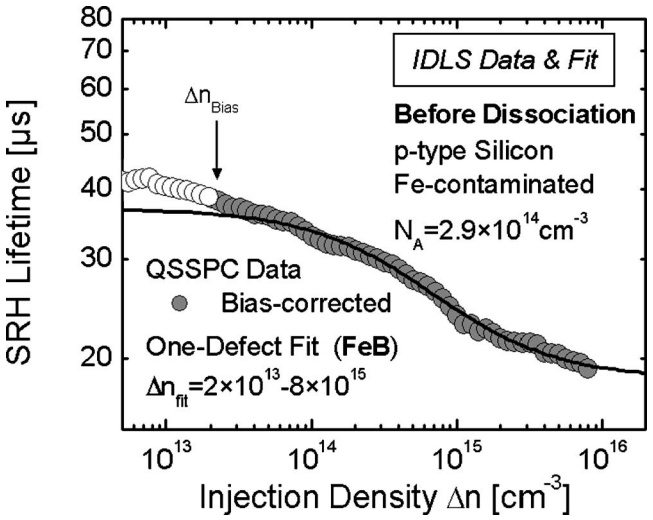

FIG. 7. SRH analysis of the FeB-dominated IDLS curve. To ensure a complete binding of interstitial Fe_i in FeB pairs, the IDLS curve is measured after a 25 h dark storage at 50 °C. Superposed carrier trapping is eliminated by means of the bias-light correction. Using an optimum bias intensity of 0.1 sun, the corrected lifetime data are reliable down to the associated bias carrier density of $\Delta n_{bias}=2\times10^{13}$ cm^{-3} (*gray circles*). An accurate SRH modeling (*line*) of the trapping-corrected IDLS curve is achieved in the whole Δn range from 2×10^{13}–10^{16} cm^{-3} for a single defect level. The associated defect parameter solution surface is shown in Fig. 8 (*solid line*).

B. Advanced IDLS analysis

As TDLS only allowed a qualitative estimate of the recombination parameters of the FeB pair, the sample has been subject to a room-temperature IDLS experiment. Since the IDLS curve displayed in Fig. 7 has been measured after an optimized dark storage for 25 h at 50 °C, complete association of FeB pairs is ensured.[9] Superposed carrier trapping has been eliminated from the measured data by means of the bias-light correction suggested in Ref. 20. The optimum correction has been achieved for a low bias intensity of 0.1 sun, which allowed the recombination lifetime to be reliably determined down to the associated bias carrier density of $\Delta n_{bias}=2\times10^{13}$ cm^{-3} (gray circles). Reflecting the recombination properties of only the FeB pair, the measured injection dependence can be accurately modeled in the whole injection range from 2×10^{13} to 10^{16} cm^{-3} assuming a single defect level, as shown in Fig. 7 by the solid line. The comprehensive spectroscopic analysis of the IDLS curve again requires the determination of the associated defect parameter solution surface. The DPSS-k curve is displayed in Fig. 8 (solid line). Again it should be emphasized that the DPSS parameter pairs (E_t,k) represent equivalent solutions for the SRH parametrization. As expected for a decreasing IDLS curve, the DPSS exhibits a split range of validity as solutions around midgap do not exist. The two energy values confining the range of validity represent characteristic quantities of the DPSS: the DPSS definition gap (DPSS-DG) in the upper half

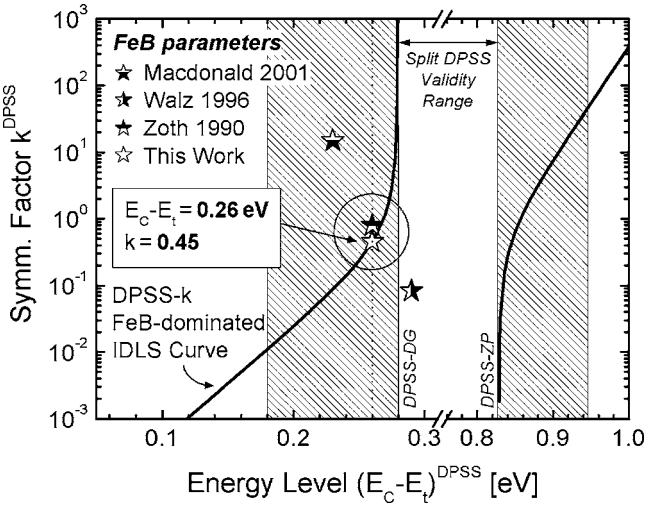

FIG. 8. Comparison of the DPSS-*k* curve associated with the FeB-dominated IDLS curve (*line*) with the FeB parameters known from the literature (Refs. 1, 12, and 13) (*filled stars*, see Table I). As being characteristic for decreasing IDLS curves, the defect parameter solution surface has a split range of validity with a definition gap around midgap. Using the spectroscopic information contained in the DPSS zero point (DPSS-ZP) allows a further confinement of the DPSS parameter solutions possible for the FeB defect (*shaded areas*). The DPSS solutions in the lower band-gap half can be excluded for reasons of consistency. Though still being ambiguous, our results suggest intermediate defect parameters for the FeB level close to the ones determined by Zoth and Bergholz (see Ref. 1). Assuming the average E_t value from the literature (Ref. 5), the optimum *k* factor may be directly extracted from the DPSS-*k* curve (*white star*).

and the DPSS zero point (DPSS-ZP) in the lower half, whose values are determined from Fig. 8 as $(E_C-E_t)^{\text{DPSS-DG}}=0.280$ eV and $(E_t-E_V)^{\text{DPSS-ZP}}=0.300$ eV. A theoretical discussion of the DPSS structure and of the spectroscopic value of its characteristics may be found in Ref. 9.

As deduced there, the energy depth $\Delta E_t^{\text{DPSS-ZP}}$ of the DPSS zero point provides additional spectroscopic information since it allows the determination of an energy interval for the unknown energy depth ΔE_t^{true} of the defect. This approach makes use of the fact that $\Delta E_t^{\text{DPSS-ZP}}$ overestimates ΔE_t^{true} by a constant amount, which only depends on the symmetry factor and the band-gap half of the defect level but not on the energy depth itself.[9] As a conservative assessment of the TDLS result still allows a *k* confinement to 0.01–1, the maximum overestimation of ΔE_t^{true} by $\Delta E_t^{\text{DPSS-ZP}}$ can directly be determined as $\Delta E^{\max}=0.12$ eV.

Thus, using the spectroscopic information contained in the DPSS-ZP, the range of possible defect energies reduces to those parts of the DPSS definition range which lie within an energy interval of 0.18–0.30 eV from either band edge, with $\Delta E_t^{\text{DPSS-ZP}}$ as upper bound and $\Delta E_t^{\text{DPSS-ZP}}-\Delta E^{\max}$ as lower bound. These intervals are displayed in Fig. 8 by the shaded areas. It becomes evident that the expanded DPSS analysis significantly narrows down the DPSS parameter solutions which, in fact, have to be taken into account for the FeB pair. While the initial DPSS-*k* curve allowed no *k* confinement at all, the symmetry factor is found to be limited to $k>0.01$ in the MinBH and to $k<50$ in the MajBH if the additional DPSS-ZP information is taken into account. Moreover, the finding of a lower bound of 0.18 eV for the defect energy depth provides further proof that the shallow FeB donor level—known to be located at $E_t-E_V=0.1$ eV—definitely has to be excluded as the dominant recombination center.

C. Comparison of the LS results with the literature and discussion

In spite of the inherent ambiguity of the IDLS results and the experimental uncertainty of the TDLS results, both techniques consistently—but indirectly—identify the deep FeB acceptor level in the upper band-gap half as the dominant recombination center. Concerning its energy level E_t, IDLS provides an energy interval of 0.18–0.28 eV below the conduction band. Though being tainted with a higher uncertainty, the E_t results from TDLS are consistent and strongly suggest the acceptor level to be located at the upper end of the E_t interval from IDLS. Concerning the symmetry factor *k*, even a conservative assessment of the TDLS results allows a *k* confinement to 0.01–1, the lower bound being confirmed by the IDLS results.

However, due to the remaining ambiguity of the IDLS results, the accurate determination of the recombination parameters of the FeB pair requires the use of a result from the literature for either the energy level or the symmetry factor. To ensure a reasonable choice, Fig. 8 shows a comparison of the IDLS results obtained in the present study (solid line) with the spectroscopic results reported in the literature (filled symbols), whose origin and limited quality have been discussed in Sec. II B. As can be seen, our results strongly suggest intermediate defect parameters for the FeB level close to the ones determined by Zoth and Bergholz.[1] As the *k* results from the literature scatter over a broad range which covers two orders of magnitude, their uncertainty exceeds by far the uncertainty observed for E_t which clearly points towards a lifetime spectroscopic determination of *k* on the basis of a chosen E_t. In a recent review,[5] an average value of $E_C-E_t=(0.26\pm0.03)$eV has been determined for the energy of the FeB acceptor level. As this value represents the best determination available to date and is fully consistent with the TDLS and IDLS results of the present study, it has been used as a basis to determine the *k* factor of the FeB acceptor level from the DPSS-*k* curve related to IDLS. As shown in Fig. 8 (white star), its optimum value is found to be $k=0.45$.

D. Additional information from the combined analysis of the FeB- and Fe_i-dominated IDLS curves

While the lifetime spectroscopic results of the present work combined with reliable σ_p results from the literature gave a complete picture of the recombination properties of the Fe_i defect (see Sec. V), the knowledge of the recombination properties of the FeB defect is still incomplete. Although the energy level and the symmetry factor of the FeB defect could be determined by means of lifetime spectroscopy, the magnitude of its capture cross sections is still unknown as the results from the literature are very inconsistent and thus scarcely reliable (see Table I). This inconsistency of the σ results is directly reflected in the strong *k* scatter observed in Fig. 8 and has been discussed in Sec. II B. Although it is in general impossible to estimate the absolute magnitude of the

capture cross sections from lifetime spectroscopy if the defect concentration is unknown, it is possible in the case of iron. Due to the fact that the iron content may be deliberately cycled between being completely present as either FeB pairs or as Fe_i ions, the combined analysis of the two associated IDLS curves provides additional information, which may be exploited in the present case of an intentionally iron-contaminated sample to determine the unknown capture cross sections of the FeB defect.

This additional spectroscopic information is contained, e.g., in the crossover position of the two IDLS curves where carrier lifetime remains unchanged upon dissociation (see Sec. IV A). If the lifetime in both defect states is expressed by the general SRH model and if both terms are equated according to the defining feature of the crossover, a general expression for the crossover position $\Delta n_{\text{crossover}}$ may be derived which only depends on the doping concentration and defect parameter triplets (E_t, k, σ_n) of the Fe_i and FeB defects. This is explicitly shown in Ref. 9. Since all these parameters except for the electron-capture cross section σ_n^{FeB} of the FeB pair are reliably known from the results obtained so far and since the crossover position itself is determined experimentally as 2×10^{13} cm^{-3} (see Fig. 1), σ_n^{FeB} as the only missing defect parameter can directly be calculated from the analytical expression for $\Delta n_{\text{crossover}}$.

As a result of this evaluation, the FeB capture cross sections are determined as $\sigma_n = 2.5\times10^{-15}$ cm^2 and $\sigma_p = 5.5\times10^{-15}$ cm^2.[9] A comparison of the σ results obtained in the present study with those from the literature shows (see Table I) that the electron-capture cross section $\sigma_n = 2.5\times10^{-15}$ cm^2 coincides with the one determined by Walz *et al.*[12] However, the hole-capture cross section $\sigma_p = 5.5\times10^{-15}$ cm^2 represents an intermediate value which is almost an order of magnitude smaller than that of Walz *et al.*[12] and slightly higher than that determined by Macdonald *et al.*[13] and Zoth and Bergholz.[1]

When assessing the quality of the spectroscopic result it is important to verify its consistency with experimental observations from the literature. While it is impossible to verify if the set of defect parameters found here for the Fe_i and the FeB defect enables an adequate SRH modeling of the IDLS curves published in the literature,[12,13] the crossover position represents a quantity which can directly be extracted from the data and easily be simulated on the basis of the parameter set found here and thus allows a simple consistency check.

As a recent study by Macdonald *et al.*[3] focused on an accurate determination of the crossover position on iron-contaminated samples with a much higher doping concentration (see Sec. IV A), these data are most relevant to verify the validity of our spectroscopic results. If $\Delta n_{\text{crossover}}$ is calculated on the basis of the set of Fe_i and FeB recombination parameters—determined here—according to the general expression given in Ref. 9, the crossover positions in the two samples of Ref. 3 are theoretically predicted at 1.4×10^{14} cm^{-3} (for $N_A = 1.5\times10^{16}$ cm^{-3}) and 2.0×10^{14} cm^{-3} (for $N_A = 2.2\times10^{16}$ cm^{-3}). Since these positions precisely coincide with the crossover positions Macdonald *et al.* determined experimentally as 1.3×10^{14} and 2.0×10^{14} cm^{-3},[3] the spectroscopic result of the present work is nicely confirmed. Moreover, as the different sets of FeB parameters known from the literature (see Table I) fail to predict the crossover at 2×10^{13} cm^{-3} in the low-doped sample of the present study, these parameter sets prove to be incorrect.[9]

It has to be concluded that the doping dependence of the crossover position is much stronger than assumed in Ref. 3. Although the crossover position is not a fixed number, its measurement still allows a fast and unambiguous identification of iron in silicon as $\Delta n_{\text{crossover}}$ may be accurately predicted for arbitrary doping concentrations. However, these calculations of $\Delta n_{\text{crossover}}$ have to be performed on the basis of the general expression given in Ref. 9, as the approximated equation given in Ref. 3 is invalid if the changed capture asymmetries of both defect centers are taken into account.

VII. CONCLUSION

The LS investigation on the iron-contaminated *p*-type sample aimed at a complete characterization of both the Fe_i and the FeB defect to verify well-known parameters and to determine others which are tainted with a high uncertainty in spite of the intensive studies on iron in the past. Facing the problem of defect transformation, both defect states have been carefully prepared in IDLS and TDLS.

Concerning the defect related to interstitial iron, the LS study unambiguously identified the Fe_i donor level in the lower band-gap half and determined its energy level as $E_t - E_V = (0.394\pm0.005)$eV and its symmetry factor as $k = 51\pm5$. The fact that two independent techniques, TDLS alone and the combination of TDLS and IDLS, led to the same spectroscopic result, demonstrates the quality and reliability of the defect parameters found. While the E_t value is in perfect agreement with the average E_t value reported in the literature—which demonstrates the excellent performance of lifetime spectroscopy—the capture asymmetry of the donor level proved to be an order of magnitude lower than determined from the capture cross sections published in the literature. Using a well-confirmed average value from the literature for the hole-capture cross section, the k factor allowed the poorly confirmed electron-capture cross section to be recalculated, which led to a room-temperature value of $\sigma_n = (3.6\pm0.4)\times10^{-15}$ cm^2. Moreover, the observed exponential $\sigma(T)$ dependence revealed that the electron capture into the Fe_i donor level is thermally activated with a barrier energy $E_\infty = 0.024$ eV, which shows that the multiphonon emission mechanism is the dominant capture mechanism not only for holes—as known from the literature—but as well for electrons.

Concerning the defect related to the iron-boron pair, the LS study unambiguously identified the deep FeB acceptor level in the upper band-gap half as the dominant recombination center. The TDLS and IDLS results being fully consistent with the average energy value of $E_C - E_t = (0.26\pm0.03)$eV known from the literature, the symmetry factor has been determined as $k = 0.45$. This k value is intermediate compared to the strongly scattered k results reported in the literature and shows that the hole capture is slightly enhanced compared to electron capture. Exploiting the addi-

tional spectroscopic information, which are provided by a combined analysis of the IDLS curves measured before (FeB dominated) and after (Fe_i dominated) pair dissociation, we were able to determine the unknown capture cross sections of the FeB defect and found $\sigma_n = 2.5 \times 10^{-15}$ cm^2 and $\sigma_p = 5.5 \times 10^{-15}$ cm^2.

Concerning the crossover position of the IDLS curves measured before and after pair dissociation, the present study provided experimental proof of a significant doping dependence. The fact that this doping dependence is accurately predicted on the basis of the parameter set found here for the Fe_i and the FeB defect further confirms the validity of the spectroscopic result and validates the use of the crossover position as a fingerprint of iron in silicon. Moreover, the study revealed an additional fingerprint of iron consisting in the qualitative change of the TDLS curve upon illumination and an S-like shape of the TDLS curve measured in the dark. Not being reported for any other contaminant, it represents a very robust criterion to unambiguously identify iron in silicon.

From an experimental point of view, the lifetime spectroscopic study on the iron-contaminated sample thus allowed a complete characterization of the Fe_i donor level and the FeB acceptor level and gave deeper insight into their recombination properties. As the most sensitive commercial technique[1] to detect and determine an iron contamination in silicon heavily relies on the Fe_i and FeB defect parameters,[3] the spectroscopic results are of special practical importance.

ACKNOWLEDGMENT

The authors would like to thank P. Lichtner and E. Tavaszi for lifetime measurements.

[1] G. Zoth and W. Bergholz, J. Appl. Phys. **67**, 6764 (1990).
[2] L. Jastrzebski, O. Milic, M. Dexter, J. Lagowski, D. DeBusk, K. Nauka, R. Witowski, M. Gordon, and E. Persson, J. Electrochem. Soc. **140**, 1152 (1993).
[3] D. H. Macdonald, L. J. Geerligs, and A. Azzizi, J. Appl. Phys. **95**, 1021 (2004).
[4] K. Graff, *Metal Impurities in Silicon-Device Fabrication*, Springer Series in Material Science Vol. 24, 2nd ed. (Springer, Berlin, 2000).
[5] A. A. Istratov, H. Hieslmair, and E. R. Weber, Appl. Phys. A **A69**, 13 (1999).
[6] S. Rein, P. Lichtner, W. Warta, and S. W. Glunz, Proceedings of the 29th IEEE Photovoltaics Specialists Conference, New Orleans, Louisiana, 2002, p. 190.
[7] S. Rein and S. W. Glunz, Appl. Phys. Lett. **82**, 1054 (2003).
[8] S. Rein and S. W. Glunz, Appl. Phys. A (submitted).
[9] S. Rein, *Lifetime Spectroscopy: A Method of Defect Characterization in Silicon for Photovoltaic Applications*, Springer Series in Material Science Vol. 85 (Springer, Heidelberg, 2005).
[10] C. H. Henry and D. V. Lang, Phys. Rev. B **15**, 989 (1977).
[11] Y. Hayamizu, T. Hamaguchi, S. Ushio, T. Abe, and F. Shimura, J. Appl. Phys. **69**, 3077 (1991).
[12] D. Walz, J.-P. Joly, and G. Kamarinos, Appl. Phys. A **62**, 345 (1996).
[13] D. Macdonald, A. Cuevas, and J. Wong-Leung, J. Appl. Phys. **89**, 7932 (2001).
[14] W. Zulehner (private communication).
[15] R. A. Sinton, A. Cuevas, and M. Stuckings, Proceedings of the 25th IEEE Photovoltaic Specialists Conference, Washington DC, USA, 1996, p. 457–460.
[16] S. W. Glunz, J. Schumacher, W. Warta, J. Knobloch, and W. Wettling, Prog. Photovoltaics **4**, 415 (1996).
[17] L. C. Kimerling and J. L. Benton, Physica B & C 116, 297 (1983).
[18] A. Kaniava, A. L. P. Rotondaro, J. Vanhellemont, U. Menczigar, and E. Gaubas, Appl. Phys. Lett. **67**, 3930 (1995).
[19] S. Rein, T. Rehrl, W. Warta, and S. W. Glunz, J. Appl. Phys. **91**, 2059 (2002).
[20] D. Macdonald, R. A. Sinton, and A. Cuevas, J. Appl. Phys. **89**, 2772 (2001).